

## LES of Cavitating Nozzle and Jet Flows

Hickel, S.; Orley, F; Mihatsch, MS; Schmidt, SJ

**DOI**

[10.1007/978-3-319-63212-4\\_16](https://doi.org/10.1007/978-3-319-63212-4_16)

**Publication date**

2018

**Document Version**

Final published version

**Published in**

Direct and Large-Eddy Simulation X

**Citation (APA)**

Hickel, S., Orley, F., Mihatsch, MS., & Schmidt, SJ. (2018). LES of Cavitating Nozzle and Jet Flows. In D. G. E. Grigoriadis, B. J. Geurts, H. Kuerten, J. Fröhlich, & V. Armenio (Eds.), *Direct and Large-Eddy Simulation X* (Vol. 24, pp. 133-139 ). (ERCOFTAC Series). Springer. [https://doi.org/10.1007/978-3-319-63212-4\\_16](https://doi.org/10.1007/978-3-319-63212-4_16)

**Important note**

To cite this publication, please use the final published version (if applicable).  
Please check the document version above.

**Copyright**

Other than for strictly personal use, it is not permitted to download, forward or distribute the text or part of it, without the consent of the author(s) and/or copyright holder(s), unless the work is under an open content license such as Creative Commons.

**Takedown policy**

Please contact us and provide details if you believe this document breaches copyrights.  
We will remove access to the work immediately and investigate your claim.

# LES of Cavitating Nozzle and Jet Flows

F. Örley, T. Trummer, M.S. Mihatsch, S.J. Schmidt and S. Hickel

## 1 Introduction

Accurate, predictive simulations of fuel injection and atomization are a key requirement for meeting future emission standards with optimized combustion processes. Fuel injection is a multi-component two-phase flow that involves complex thermodynamics and fluid dynamics phenomena at different spatial and temporal scales. Atomization and vaporization are influenced by the chamber conditions (pressure, temperature and velocity) and very sensitive on the properties of the fuel jet conditioned by the injector. The highly unsteady and turbulent fuel flow inside the injector involves very energetic secondary flow structures (vortices). Current trends towards higher rail pressures lead directly to larger pressure differences and promote cavitation, that is, the local evaporation and subsequent implosion-like re-condensation of fuel in throttles, at the nozzle inlets, and in vortex cores of the secondary flow structures. Both phenomena are highly sensitive on the injector geometry and strongly affect the primary atomization.

Direct interphase resolving simulations (see [5], e.g.) of practically relevant injection processes are computationally intractable, today and in the next decades. Current state-of-the-art spray simulations therefore use computationally efficient Lagrangian particle tracking (LPT) methods, which do not attempt to capture, by design, the primary breakup of the liquid fuel jet. Engineers can calibrate LPT methods in such a

---

F. Örley · T. Trummer · M.S. Mihatsch · S.J. Schmidt · S. Hickel  
Institute of Aerodynamics and Fluid Mechanics, Technische Universität München,  
Boltzmannstr. 15, 85748 Garching bei München, Germany

S. Hickel (✉)

Faculty of Aerospace Engineering, Delft University of Technology, Kluyverweg 1,  
2629 HS Delft, The Netherlands  
e-mail: s.hickel@tudelft.nl; sh@tum.de

way that they reproduce experimentally determined spray characteristics with sufficient accuracy for full-scale combustion simulations. However, LPT methods are not designed to predict the effect of new injector geometries or modified operating conditions on the spray formation. Computational spray design requires sufficiently detailed numerical methods and physical models that can accurately predict the effects of the nozzle geometry and internal nozzle flow on the primary jet breakup and downstream spray evolution. At the same time, the methods and models must be as simple as possible and have minimum computational resource requirements to enable their application in the engineering design process. The most suitable approach is to combine Eulerian large-eddy simulation (LES) of injector flow and primary jet breakup with LPT for secondary atomization and vaporization. The LES can lead to an improved understanding of the nozzle spray interaction and provide input data for LPT in regions where liquid filaments become too small to be captured on reasonable grids.

We have developed a computationally very efficient method for the LES of injector and jet flows based on an Eulerian description with barotropic phase-equilibrium models. This new model extends our compressible framework for LES of turbulent multiphase fuel flows (fuel in a liquid and gaseous state), see, e.g., Hickel et al. [3] and Egerer et al. [1], and can now additionally capture the mixing of cavitating fuel jets with non-condensable gas [7]. In this paper, we discuss selected results from recently performed LES for the cavitating nozzle and jet flow experiment of Sou et al. [9, 10]. We consider three operating points with different cavitation characteristics and identify the main mechanisms that affect the primary jet breakup.

## 2 Numerical Model

The fluid considered in this work consists of three components, liquid water ( $W$ ), water-vapor mixtures ( $M$ ), and air as non-condensable gas ( $G$ ). The flow of this fluid is governed by the compressible Navier–Stokes equations, which we discretize with the finite-volume LES model of Hickel et al. [2–4], and an additional transport equation for the mass fraction  $\beta_G$  of the non-condensable gas. We believe that it is essential to consider compressibility of all phases in order to capture cavitation induced wave dynamics. In this fully Eulerian, compressible, finite-volume framework, the transported volume-averaged mass density  $\rho = \sum_{\phi} \beta_{\phi} \rho_{\phi}$ , is the sum of the volume-averaged densities  $\rho_{\phi}$  of the three components  $\Phi = \{M, W, G\}$  weighted by their volume fraction  $\beta_{\phi}$ . By assuming thermodynamic and mechanical equilibrium, the cell-averaged pressure  $p$  can be computed from the equations of state (EOS) of the individual components  $\Phi = \{M, W, G\}$  to close the transport equations. In this work, we use barotropic equations of state, leading to  $p = p(\rho, \beta_G)$ . An isothermal, ideal gas EOS  $\rho_G = p/(R_G T_{ref})$ , with  $T_{ref} = 293.15$ , is used for the non-condensable gas. Liquid water is modeled as an isentropic fluid with a constant speed of sound  $c_{liq} = 1482.35$  m/s at the same ambient conditions. The EOS then directly follows from  $c_{liq}^2 = \partial p / \partial \rho$  by integration. This simple model is in excellent

agreement with more accurate EOS for  $p \leq 200$  bar. The same EOS framework,  $\rho = \rho_{s,liq} + (p - p_s)/c^2$ , is used to model the formation of vapor and liquid-vapor mixtures. Suitable reference conditions are the saturation pressure  $p_s$  and saturation density  $\rho_{s,liq}$  of liquid water. For  $p > p_s$ , i.e., pure liquid water, the speed of sound is  $c = c_{liq}$ . For  $p < p_s$ , i.e., two-phase liquid-vapor mixtures, we use a numerical value of  $c = c_M = 1$  m/s as conservative upper estimate of the average of the speed of sound between a frozen and an equilibrium isentropic phase change.

This thermodynamic model assumes that phase change is fast compared to the hydrodynamic time scales and in thermodynamic and mechanical equilibrium. That is, there is only one velocity field; gas, liquid and vapor have the same (thermodynamic equilibrium) pressure and surface tension is neglected. The cavitation model has been extensively applied and validated, e.g., for LES of turbulent wall-bounded flows [1, 3], for closing control valves [6], and for the cavitating flow inside a 9-hole Diesel injector during a full injection cycle [8]. For a detailed description of the model we refer to our journal paper [7].

### 3 Test Setup

Sou et al. [9, 10] have performed a series of experiments for a simplified injector geometry with an optically accessible rectangular nozzle. The experimental operating points have different mean streamwise liquid velocity  $U_N$  inside the nozzle, leading to different cavitation numbers

$$\sigma = \frac{p_\infty - p_s}{0.5\rho_L U_N^2}, \quad (1)$$

where  $p_\infty = 1$  atm =  $1.01325 \times 10^5$  Pa corresponds to the surrounding pressure, and  $\rho_L$  is the liquid density. In the following, we discuss LES results for three operation conditions: the first case with  $\sigma = 1.27$  shows no cavitation; small cavitation regions are developing inside the nozzle for the second case with  $\sigma = 0.78$ ; and supercavitation and a choked nozzle is observed for  $\sigma = 0.65$ .

Figure 1 shows the geometry and dimensions of the computational domain, which is meshed with an adaptive, locally refined Cartesian grid with a total number of  $43 \times 10^6$  cells. The mesh is strongly refined within the boundary layers and the jet region. A large, coarsely meshed plenum is added on the right, which ensures that there are no artificial interactions with outflow boundary conditions, where we impose a constant pressure of  $p_\infty = 1$  atm. The inflow boundary condition on the left is a laminar duct flow. Adiabatic no-slip wall boundary conditions are used on the top, bottom and sides.

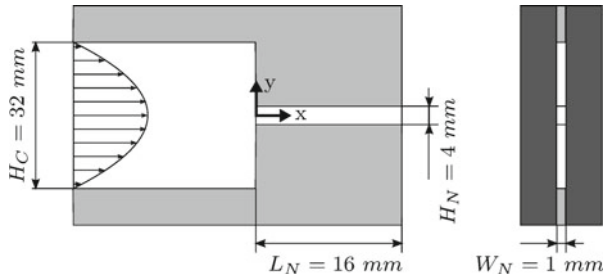


**Fig. 1** Geometry of the computational domain. The flow is from left to right. The inflow duct has a width of  $W_N = 1$  mm and a height of  $H_C = 32$  mm. The rectangular nozzle has the length  $L_N = 16$  mm, height  $H_N = 4$  mm, and width  $W_N = 1$  mm. The jet flow exits into a very large plenum on the right

## 4 Results

Instantaneous cavitation structures have been experimentally recorded as transmitted light images, which we compare with visualizations of the spanwise-integrated vapor volume fraction for three corresponding LES simulations in Fig. 2. The agreement between experiment and simulation is very good for the operating points with  $\sigma = 1.27$  and  $\sigma = 0.78$ . The effect of cavitation damping coherent turbulence structures can be observed in Fig. 3. For the third operating point with  $\sigma = 0.65$ , we observe cavitation in stable vortices that develop from the corners to the nozzle center and strongly damp the turbulence. These vortices are not stable in the experiment, probably due to a high level of inflow perturbations, cf. discussion in Ref. [7].

Cavitation has a strong effect on the liquid-jet breakup; visualizations of the jet structure are presented in Fig. 4. The two lower cavitation numbers,  $\sigma = 1.27$  and  $\sigma = 0.78$ , show a similar jet structure. The supercavitation case,  $\sigma = 0.65$ , shows a strongly increased jet angle, a much rougher jet surface and small detached liquid ligaments. The collapse of cavitation structures near the nozzle exit induces turbu-

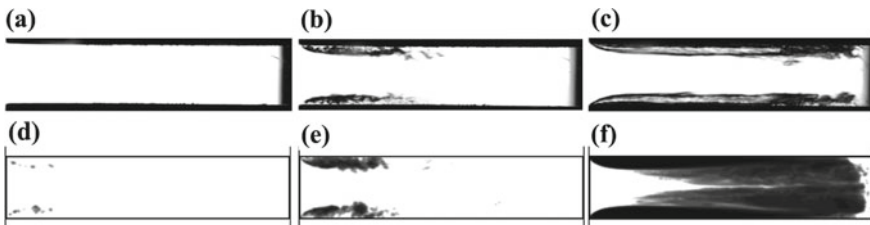


**Fig. 2** Effect of cavitation number on vapor structures inside the nozzle for three cavitation numbers: The *top* row shows transmitted-light images from Sou et al. [9] for cavitation number **a**  $\sigma = 1.27$ , **b**  $\sigma = 0.78$ , and **c**  $\sigma = 0.65$  (reprinted with permission from Elsevier). The *bottom* row (**d/e/f**) shows corresponding contours of the spanwise-averaged vapor fraction from our LES (adopted from Örley et al. [7])

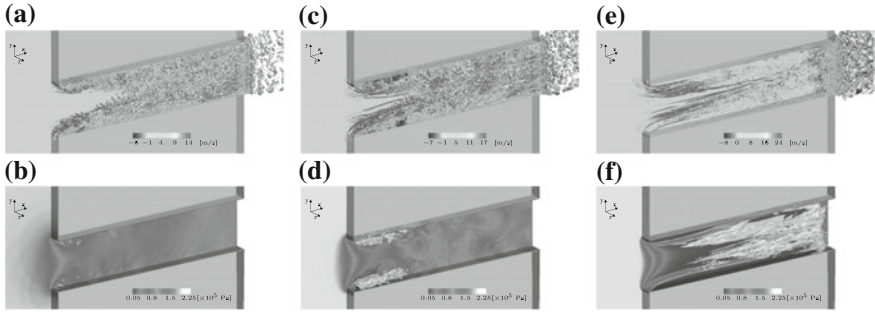


**Fig. 3** Effect of cavitation on the turbulent nozzle flow for three cavitation numbers: **a/b**  $\sigma = 1.27$ , **c/d**  $\sigma = 0.78$ , and **e/f**  $\sigma = 0.65$ . The *top* row shows iso-surfaces of  $\lambda_2 = -1 \times 10^8 \text{ 1/s}^2$ , visualizing instantaneous turbulent flow structures. The *bottom* row shows  $\alpha = 0.1$  vapor volume-fraction iso-surfaces at the same instants in time. The walls are colored by pressure contours

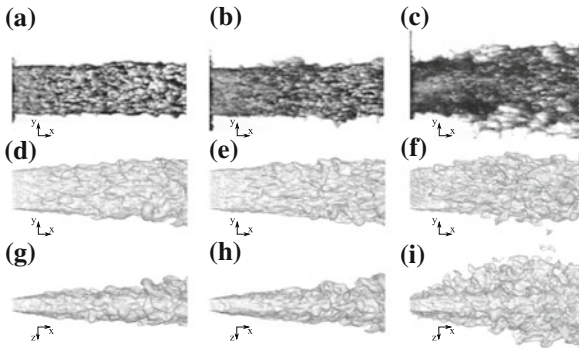


**Fig. 4** Effect of cavitation on the liquid-jet breakup for three cavitation numbers: The *top* row shows transmitted-light images from the experiment of Sou et al. [9] for cavitation number **a**  $\sigma = 1.27$ , **b**  $\sigma = 0.78$ , and **c**  $\sigma = 0.65$  (reprinted with permission from Elsevier). Corresponding snapshots of  $\beta_G = 0.99$  iso-surfaces from our simulations are shown in the center (view on  $x$ - $y$  plane) and *bottom* row (view on  $x$ - $z$  plane)

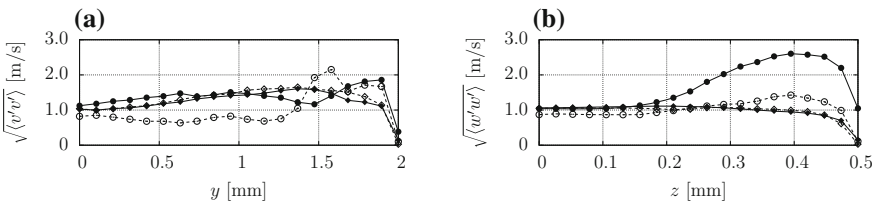


**Fig. 5** Wall-normal velocity fluctuations at the nozzle outlet at  $x = 15.0 \text{ mm}$  (*empty symbols/dashed lines*) and  $x = 16.0 \text{ mm}$  (*filled symbols/solid lines*) for  $\sigma = 0.78$  ( $\diamond$ ) and  $\sigma = 0.65$  ( $\circ$ )

lent fluctuations and promotes the jet breakup. Figure 5 shows LES results for the wall-normal velocity fluctuations in  $y$ - and  $z$ -direction,  $v'$  and  $w'$ . We see that the velocity fluctuations in  $y$ -direction,  $v'$ , increase only slightly near the top wall, Fig. 5a, however, the velocity fluctuations in  $z$ -direction,  $w'$ , increases significantly for the case with the lowest cavitation number  $\sigma = 0.65$ , see Fig. 5b, with an increase of approximately 150% compared to  $\sigma = 0.78$ .

## 5 Summary and Outlook

We have presented an Eulerian three-component two-phase model for the large-eddy simulation (LES) of the cavitating flow within liquid-fuel injectors and the primary breakup of injected fuel jets. The model was applied to a generic nozzle and jet flow at different cavitation numbers and Reynolds numbers, and correctly reproduced experimentally observed cavitation effects. We found that collapse events near the exit plane of the nozzle increase the turbulence level, perturb the liquid-gas interface, and enhance the jet breakup in very good agreement with experimental data. We subsequently identified two additional mechanisms that affect the jet breakup: The collapse of cavitation structures near the nozzle exit can lead to an entrainment of ambient gas into the nozzle, which then changes the effective nozzle cross section and tilts the jet. The collapse cavitation structures inside the jet near the liquid-gas interface leads to ejections of fuel into the ambient air, which increases the jet spreading angle. These mechanisms are discussed in more detail in Örley et al. [7].

**Acknowledgements** Computing time was granted by the Leibnitz Supercomputing Centre (LRZ) of the Bavarian Academy of Sciences and Humanities.

## References

1. Egerer, C.P., Hickel, S., Schmidt, S.J., Adams, N.A.: Large-eddy simulation of turbulent cavitating flow in a micro channel. *Phys. Fluids* **26**(8), 085102 (2014)
2. Hickel, S., Adams, N.A., Domaradzki, J.A.: An adaptive local deconvolution method for implicit LES. *J. Comput. Phys.* **213**(1), 413–436 (2006)
3. Hickel, S., Mihatsch, M., Schmidt, S.J.: Implicit large eddy simulation of cavitation in micro channel flows. In: Proceedings of the WIMRC 3rd International Cavitation Forum, University of Warwick, UK (2011)
4. Hickel, S., Egerer, C., Larsson, J.: Subgrid-scale modeling for implicit large eddy simulation of compressible flows and shock-turbulence interaction. *Phys. Fluids* **26**(10), 106101 (2014)
5. Lauer, E., Hu, X.Y., Hickel, S., Adams, N.A.: Numerical modelling and investigation of symmetric and asymmetric cavitation bubble dynamics. *Comput. Fluids* **69**, 1–19 (2012)
6. Örley, F., Pasquariello, V., Hickel, S., Adams, N.A.: Cut-element based immersed boundary method for moving geometries in compressible liquid flows with cavitation. *J. Comput. Phys.* **283**(C), 1–22 (2015)

7. Órley, F., Trummer, T., Hickel, S., Mihatsch, M.S., Schmidt, S.J., Adams, N.A.: Large-eddy simulation of cavitating nozzle flow and primary jet break-up. *Phys. Fluids* **27**(8), 086101 (2015)
8. Órley, F., Hickel, S., Schmidt, S.J., Adams, N.A.: Large-eddy simulation of turbulent, cavitating flow inside a 9-hole Diesel injector including needle movement. *Int. J. Engine Res.* **18**, 195–211 (2017)
9. Sou, A., Hosokawa, S., Tomiyama, A.: Effects of cavitation in a nozzle on liquid jet atomization. *Int. J. Heat Mass Transf.* **50**, 3575–3582 (2007)
10. Sou, A., Tomiyama, A., Hosokawa, S., Nigorikawa, S., Maeda, T.: Cavitation in a two-dimensional nozzle and liquid jet atomization. *JSME Int. J. Ser. B, Fluids Thermal Eng.* **49**(4), 1253–1259 (2006)